

Influence of Material Toughness on Fracture Reliability in Steel Bridges

November 2018



U.S. Department of Transportation
Federal Highway Administration

Sponsored by

Federal Highway Administration
Office of Infrastructure
FHWA-HIF-18-047

Foreword

This report documents a study on the influence of base material toughness on the structural reliability of highway bridges with steel primary members, with focus on the fracture limit state. It is well-known that modern bridge steels are produced with improved toughness properties as compared to legacy materials. However the benefits of this improved toughness related to reliability have until now not been quantified. This work established a quantified relationship between material toughness properties and reliability which might be considered in a risk-based approach to bridge inspection and management.

The hard and competent work of Modjeski and Masters, Inc. and Lehigh University in performing this research and producing this report is gratefully acknowledged.

A handwritten signature in black ink, appearing to read 'J. Hartmann', with a long horizontal flourish extending to the right.

Joseph L. Hartmann, PhD, P.E.
Director, Office of Bridges and Structures
Office of Infrastructure
Federal Highway Administration

Notice

This document is disseminated under the sponsorship of the U.S. Department of Transportation in the interest of information exchange. The U.S. Government assumes no liability for the use of the information contained in this document.

The U.S. Government does not endorse products or manufacturers. Trademarks or manufacturers' names appear in this report only because they are considered essential to the objective of the document.

Quality Assurance Statement

The Federal Highway Administration (FHWA) provides high-quality information to serve Government, industry, and the public in a manner that promotes public understanding. Standards and policies are used to ensure and maximize the quality, objectivity, utility, and integrity of its information. FHWA periodically reviews quality issues and adjusts its programs and processes to ensure continuous quality improvement.

TECHNICAL REPORT DOCUMENTATION PAGE

1. Report No. FHWA-HIF-18-047	2. Government Accession No.	3. Recipient's Catalog No.	
4. Title and Subtitle Influence of Material Toughness on Fracture Reliability in Steel Bridges		5. Report Date October 2018	
		6. Performing Organization Code:	
7. Author(s) Frank A. Artmont, Thomas P. Murphy, Richard Sause, Paolo Bocchini, and Dennis Mertz		8. Performing Organization Report No.	
9. Performing Organization Name and Address Modjeski and Masters, Inc. 100 Sterling Parkway, Suite 302 Mechanicsburg, PA 17050 ATLSS Engineering Research Center at Lehigh University 117 ATLSS Drive Bethlehem, PA 18015		10. Work Unit No.	
		11. Contract or Grant No. DTFH61-11-H-00027	
12. Sponsoring Agency Name and Address Federal Highway Administration Office of Infrastructure – Bridges and Structures 1200 New Jersey Ave., SE Washington, DC 20590		13. Type of Report and Period Covered Final Report August 2017 to September 2018	
		14. Sponsoring Agency Code	
15. Supplementary Notes Work funded by Cooperative Agreement "Advancing Steel and Concrete Bridge Technology to Improve Infrastructure Performance" between FHWA and Lehigh University. FHWA Technical Manager: Brian M. Kozy			
16. Abstract The AASHTO LRFD Bridge Design Specifications do not explicitly include a quantifiable fracture limit state. Fracture control in steel bridges is currently based on mitigating potential fracture initiators through proper structural detailing and specifying minimum impact toughness for base material. This fracture control approach has been successful in minimizing the number of fractures in steel bridges designed since its inception; however, the structural reliability against brittle fracture has not been previously established. Accordingly, the objective of this study is to quantify the relationship between material toughness and fracture reliability in steel bridge members, considering the probabilistic distribution of fracture toughness and applied stress for a variety of structural steels and assumed crack sizes. The master curve approach is used to account for the probabilistic distribution of fracture toughness, and reliabilities are determined using Monte Carlo simulation and the Hasofer-Lind approach. The results indicate that the fracture reliability for modern bridge steels is consistent with the reliability of AASHTO strength limit states, and that certain steels currently available on the market can provide enough reliability against fracture to essentially eliminate brittle fracture as a limit state of concern.			
17. Key Words Steel bridges, fatigue, fracture, reliability, Monte Carlo simulation		18. Distribution Statement No restrictions. This document is available through the National Technical Information Service, Springfield, VA 22161.	
19. Security Classif. (of this report) Unclassified	20. Security Classif. (of this page) Unclassified	21. No. of Pages 46	22. Price Free

Form DOT F 1700.7 (8-72)

Reproduction of completed page authorized.

SI* (MODERN METRIC) CONVERSION FACTORS

APPROXIMATE CONVERSIONS TO SI UNITS

Symbol	When You Know	Multiply By	To Find	Symbol
LENGTH				
in	inches	25.4	millimeters	mm
ft	feet	0.305	meters	m
yd	yards	0.914	meters	m
mi	miles	1.61	kilometers	km
AREA				
in ²	square inches	645.2	square millimeters	mm ²
ft ²	square feet	0.093	square meters	m ²
yd ²	square yard	0.836	square meters	m ²
ac	acres	0.405	hectares	ha
mi ²	square miles	2.59	square kilometers	km ²
VOLUME				
fl oz	fluid ounces	29.57	milliliters	mL
gal	gallons	3.785	liters	L
ft ³	cubic feet	0.028	cubic meters	m ³
yd ³	cubic yards	0.765	cubic meters	m ³
NOTE: volumes greater than 1000 L shall be shown in m ³				
MASS				
oz	ounces	28.35	grams	g
lb	pounds	0.454	kilograms	kg
T	short tons (2000 lb)	0.907	megagrams (or "metric ton")	Mg (or "t")
TEMPERATURE (exact degrees)				
°F	Fahrenheit	5 (F-32)/9 or (F-32)/1.8	Celsius	°C
ILLUMINATION				
fc	foot-candles	10.76	lux	lx
fl	foot-Lamberts	3.426	candela/m ²	cd/m ²
FORCE and PRESSURE or STRESS				
lbf	poundforce	4.45	newtons	N
lbf/in ²	poundforce per square inch	6.89	kilopascals	kPa

APPROXIMATE CONVERSIONS FROM SI UNITS

Symbol	When You Know	Multiply By	To Find	Symbol
LENGTH				
mm	millimeters	0.039	inches	in
m	meters	3.28	feet	ft
m	meters	1.09	yards	yd
km	kilometers	0.621	miles	mi
AREA				
mm ²	square millimeters	0.0016	square inches	in ²
m ²	square meters	10.764	square feet	ft ²
m ²	square meters	1.195	square yards	yd ²
ha	hectares	2.47	acres	ac
km ²	square kilometers	0.386	square miles	mi ²
VOLUME				
mL	milliliters	0.034	fluid ounces	fl oz
L	liters	0.264	gallons	gal
m ³	cubic meters	35.314	cubic feet	ft ³
m ³	cubic meters	1.307	cubic yards	yd ³
MASS				
g	grams	0.035	ounces	oz
kg	kilograms	2.202	pounds	lb
Mg (or "t")	megagrams (or "metric ton")	1.103	short tons (2000 lb)	T
TEMPERATURE (exact degrees)				
°C	Celsius	1.8C+32	Fahrenheit	°F
ILLUMINATION				
lx	lux	0.0929	foot-candles	fc
cd/m ²	candela/m ²	0.2919	foot-Lamberts	fl
FORCE and PRESSURE or STRESS				
N	newtons	0.225	poundforce	lbf
kPa	kilopascals	0.145	poundforce per square inch	lbf/in ²

*SI is the symbol for the International System of Units. Appropriate rounding should be made to comply with Section 4 of ASTM E380.
(Revised March 2003)

TABLE OF CONTENTS

INTRODUCTION.....	1
METHODOLOGY	3
LIMIT STATE EQUATION	3
FRACTURE TOUGHNESS	3
STRESS INTENSITY FACTORS	6
APPLIED STRESSES	8
MONTE CARLO SIMULATION.....	8
RESULTS	11
MASTER CURVE REFERENCE TEMPERATURE	11
RELIABILITY BY MATERIAL GRADE.....	11
RELIABILITY BY CRACK TYPE AND MATERIAL THICKNESS.....	15
ADDITIONAL SIMULATIONS FOR LARGE TOUGHNESS STEEL.....	19
CONCLUSIONS	25
REFERENCES.....	27

LIST OF FIGURES

Figure 1. Equation. Limit state equation for fracture failure.	3
Figure 2. Equation. Empirical master curve equation.....	3
Figure 3. Graph. Example fracture toughness master curves.	4
Figure 4. Equation. Relationship between reference temperature and 27J temperature.....	4
Figure 5. Graph. CVN test results for legacy ASTM A242 steel.	5
Figure 6. Equation. Reference temperature shift for loading rate effects.....	6
Figure 7. Equation. Additional loading rate equation parameter.....	6
Figure 8. Equation. Stress intensity factor.	6
Figure 9. Illustration. Assumed cracks: (a) through-thickness, and (b) semi-elliptical.....	7
Figure 10. Equation. Stress intensity correction factor.....	7
Figure 11. Equation. Back surface correction factor.	7
Figure 12. Equation. Elliptical flaw shape parameter.....	7
Figure 13. Graph. Variability in fracture toughness at -30°F for legacy and modern steels.	12
Figure 14. Graph. Simulation results for a legacy ASTM A242 steel.....	12
Figure 15. Graph. Simulation results for a legacy ASTM A572 steel.....	13
Figure 16. Graph. Simulation results for a modern ASTM A709-50 steel.....	13
Figure 17. Graph. Simulation results for a modern ASTM A709-50W steel.	14
Figure 18. Graph. Simulation results for a modern ASTM A709-HPS50W steel.....	14
Figure 19. Graph. Simulation results for semi-elliptical crack in 1-inch thick component.....	16
Figure 20. Graph. Simulation results for semi-elliptical crack in 2.5-inch thick component.....	16
Figure 21. Graph. Simulation results for through-thickness crack in 1-inch thick component. ...	17
Figure 22. Graph. Simulation results for through-thickness crack in 2.5-inch thick component. ...	17
Figure 23. Equation. General form of limit state function for Hasofer-Lind approach.....	19
Figure 24. Equation. General form of the Hasofer-Lind reliability index.....	19
Figure 25. Equation. Hasofer-Lind reliability index for uncorrelated random variables.	20
Figure 26. Equation. Hasofer-Lind reliability index for fracture limit state function.	20
Figure 27. Graph. Hasofer-Lind reliability analysis results for modern A709/A572 low carbon microalloyed steel compared with modern A709-50 Monte Carlo simulation results.	21
Figure 28. Graph. Variability in fracture toughness at -30°F for all considered materials.....	22
Figure 29. Graph. Variability in fracture toughness at -30°F for synthetic/fictitious steels, compared to variability for A709/A572 low C steel.....	22
Figure 30. Graph. Reliability index vs. critical crack size for synthetic materials.	23
Figure 31. Graph. Critical crack size vs. lower bound fracture toughness for β of 3.5	23

LIST OF TABLES

Table 1. Normal distribution parameters for applied stresses.....	8
Table 2. Master curve reference temperatures for selected materials.....	11
Table 3. Maximum crack size (a) for target reliability index of 3.5.....	15

LIST OF ABBREVIATIONS

AASHTO	American Association of State Highway and Transportation Officials
ASTM	American Society for Testing and Materials
AWS	American Welding Society
COV	Coefficient of Variation
CVN	Charpy V-Notch
DL	Dead Load
FHWA	Federal Highway Administration
HL	Hasofer-Lind
LAST	Lowest Anticipated Service Temperature
LEFM	Linear Elastic Fracture Mechanics
LL	Live Load
LRFD	Load and Resistance Factor Design
M&M	Modjeski and Masters
MC	Master Curve
MCS	Monte Carlo Simulation
NBIS	National Bridge Inspection Standards

INTRODUCTION

The Federal Highway Administration (FHWA) provides assurance of bridge safety by enforcement of the National Bridge Inspection Standards (NBIS), which are defined in the Code of Federal Regulations. The NBIS dictate that Fracture Critical steel members must receive a biennial “hands-on” inspection.¹ This requirement is intended to mitigate the risk to the structure that may be created by the occurrence of a fracture in the member, which may occur as the result of a developing fatigue crack. This approach to fracture risk mitigation has its origins when steel materials were much less resistant to fracture and no bridge inspection or management standards were in place.

More recently, FHWA has developed new policies for bridge management that are based on risks to the structure. In general, risk can be considered as the product of probability of failure times the consequence of failure. In the context of fracture risk, the material toughness has a direct impact on the probability of fracture, which also affects the risk. The FHWA initiated this project to develop a deeper understanding of fracture risk by applying structural reliability theory and quantifying the influence on fracture risk from changes to material toughness.

The AASHTO LRFD Bridge Design Specifications⁽¹⁾ do not explicitly include a fracture limit state. The specifications provide provisions for fracture control in steel bridges based on (a) minimizing the number of potential fracture initiation points present in a bridge through the prescription of good detailing practices with adequate fatigue design provisions and (b) specifying a required material impact toughness based on the temperature zones defined by the specifications. These requirements depend on the type of steel, thickness of the plate, the temperature zone, and whether the member is fracture-critical or not. This fracture control plan has been successful in minimizing the number of fractures in steel bridges designed since its inception; however, the structural reliability against a failure caused by tension fracture has not been previously established. In contrast, the load and resistance factors for the strength limit states of the AASHTO specifications have been calibrated so that the target reliability index of the specifications is 3.5, corresponding to a target failure rate of 1 in 5000 or failure probability of 0.02% over the 75-year life of a bridge.

The objective of this study is to quantify the relationship between material toughness and fracture reliability in steel bridge members, considering the probabilistic distribution of fracture toughness and applied stress for a variety of structural steels and assumed crack sizes. The specific goals include (1) the development of a limit state equation for bridge member fracture, (2), the quantification of fracture reliability considering the variability in parameters, and (3) the calculation of changes in fracture reliability related to material toughness and crack size.

¹ 23 CFR 650.311(c)

METHODOLOGY

LIMIT STATE EQUATION

To quantify the reliability of steel bridges against fracture failure, a limit state equation is required that relates the applied demand to the supplied resistance. For a given stress state, crack geometry, and set of material characteristics, the maximum flaw size a structural member can tolerate without unstable crack propagation can be calculated using the principles of Linear Elastic Fracture Mechanics (LEFM) by setting the applied stress intensity, i.e., the applied demand, equal to the material's fracture toughness, i.e., the supplied resistance. In mathematical form, this limit state function is presented in Figure 1.

$$g = K_C - K_I$$

Figure 1. Equation. Limit state equation for fracture failure.

In this equation, K_C is the fracture toughness of the material containing the flaw, and K_I is the stress intensity factor dependent on the applied stress, flaw size, and geometry. When g is less than zero, unstable fracture of the member may occur. The use of LEFM provides a conservative limit state function (due to its plane-strain assumption) that is easily applicable for design purposes.

FRACTURE TOUGHNESS

For the purposes of this study, the fracture toughness is defined using the Master Curve (MC) approach. The MC is an empirical equation that allows the determination of the statistical distribution of fracture toughness at any desired temperature throughout the lower shelf and transition regions of the fracture toughness vs. temperature relationship. The applicability of this approach to modern and legacy bridge steels has been demonstrated previously. ⁽²⁾ The MC describes the variation in fracture toughness with temperature, while also providing a probabilistic distribution of the fracture toughness at a given temperature for a given material. Before discussing the MC equation, it should be noted that the equation and many of its modifying equations (such as for loading rate effects discussed later) are empirical and are provided for the SI unit system only. The empirical MC equation for ferritic metals in SI units is given in Figure 2.

$$K_C = 20 + [11 + 77e^{(0.019(T-T_o)}] \left[\frac{25}{B} \right]^{0.25} \left[\ln \left(\frac{1}{1 - P_f} \right) \right]^{0.25}$$

Source: Reference 6

Figure 2. Equation. Empirical master curve equation.

In this equation, K_C is the fracture toughness (MPa-√m), T is the service temperature (°C), T_o is an experimentally-determined reference temperature (°C) that corresponds to the median fracture toughness of 100 MPa-√m for a given material, B is the thickness of the plate for a through-thickness flaw (mm), and P_f is the cumulative probability of failure or fracture toughness

percentile, i.e. the likelihood that the true fracture toughness is below the calculated value. To demonstrate the basics of the master curve, the fracture toughness master curves at a reference temperature of -76 °F are plotted in Figure 3 for varying degrees of fracture toughness percentile. The master curves predict larger scatter at temperatures near the transition region, and smaller scatter for lower temperatures on the lower shelf.

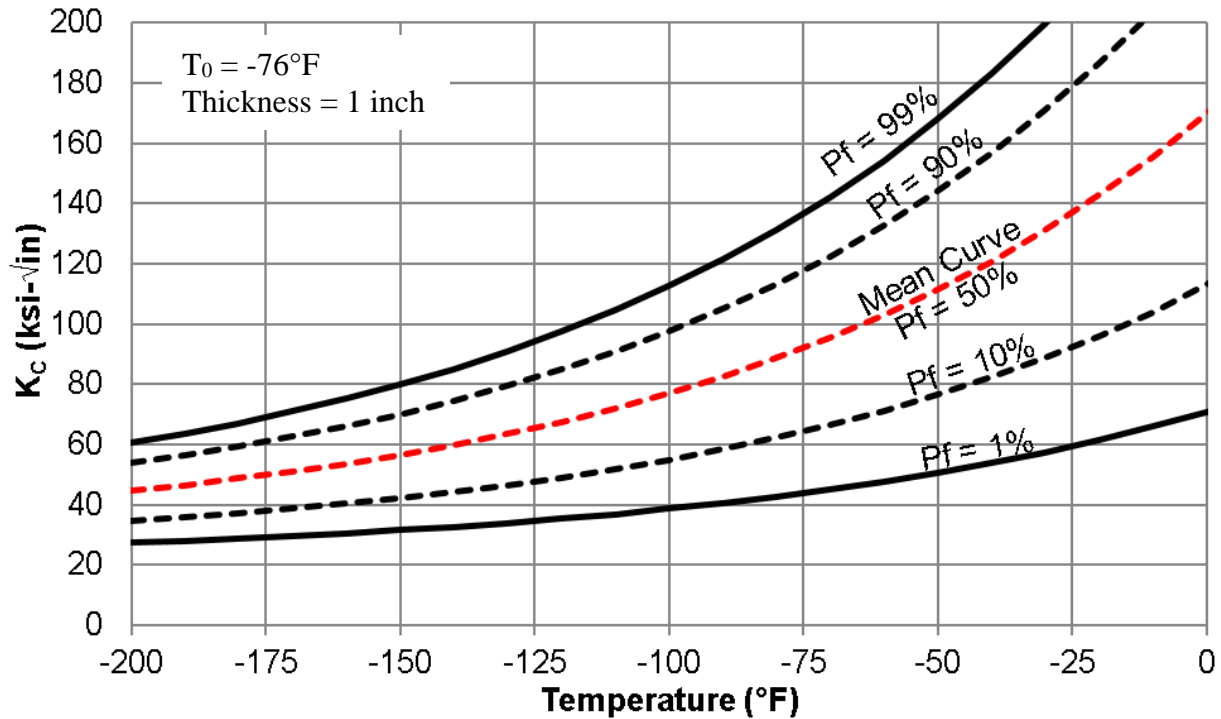


Figure 3. Graph. Example fracture toughness master curves.

The reference temperature can be approximated from CVN impact toughness data using the relationship presented in Figure 4. In this equation, T_{27J} is the temperature (°C) at which the CVN impact energy was equal to 27 J (20 ft-lb).

$$T_o = T_{27J} - 18$$

Source: Reference 6

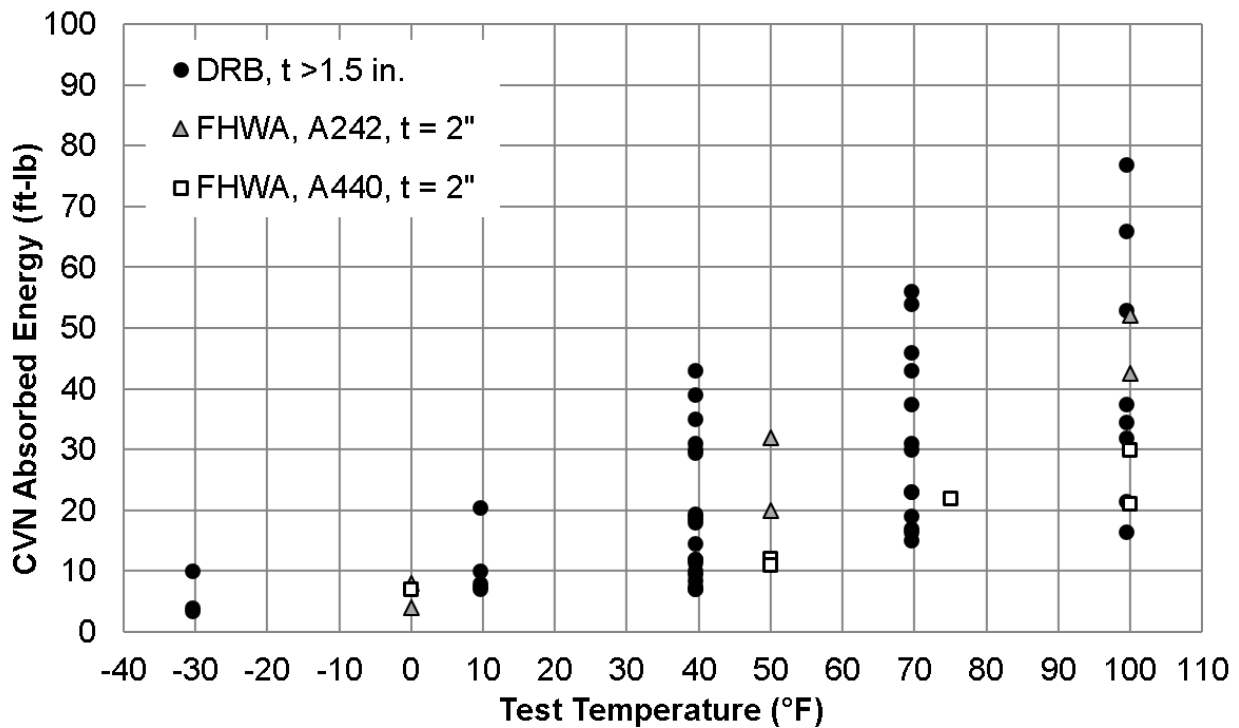
Figure 4. Equation. Relationship between reference temperature and 27J temperature.

To determine the reference temperature for each material, the average of the CVN values at each temperature were determined. These averages were plotted, and the T_{27J} temperature was determined from these values (and their associated temperatures) by linear interpolation. Predicted T_o values were then calculated using the above correlation equation.

The reference temperatures for a total of six different materials were calculated as part of this study. These included the following legacy and modern steels:

- Legacy ASTM A242
- Legacy ASTM A572 Grade 50
- Modern ASTM A709 Grade 50
- Modern ASTM A709 Grade 50W
- Modern ASTM A709 HPS50W

For ASTM A242 steel, CVN data was taken from a recent material testing program for a legacy truss bridge⁽³⁾ that incorporated more than 200 CVN tests from material of various thicknesses. This data was compared to available data for similar ASTM A242 steel from the same era⁽⁴⁾, and found to be in general agreement, as shown in Figure 5.



Source: Reference 3, Reference 4

Figure 5. Graph. CVN test results for legacy ASTM A242 steel.

For ASTM A572 steel, CVN data was extracted from an article by Barsom⁽⁵⁾, which formed the basis for the original AASHTO fracture-toughness requirements for bridge steels.

For the modern steels, CVN data was provided by two steel producers who preferred to remain anonymous and to keep their CVN data anonymous. The CVN plots for these three data sets looked like typical CVN plots for structural steel. One important observation from these plots is that the data for the non-HPS grades tended to be higher than for the HPS grade, even if all steels passed the AASHTO CVN requirements. This is a consequence of the large range of allowable chemistries in ASTM A709, and different producers using their own proprietary processes and chemistries to achieve their desired properties.

The Wallin MC was also modified for a bridge loading rate by using a shift of the reference temperature⁽⁶⁾ as shown in Figure 6.

$$\Delta T_0 = \frac{(T_{01} + 273) \ln \left(\frac{dK_c}{dt} \right)}{\Gamma - \ln \left(\frac{dK_c}{dt} \right)}$$

Source: Reference 6

Figure 6. Equation. Reference temperature shift for loading rate effects.

In this equation, ΔT_0 is the shift of reference temperature due to loading rate effects (°C), T_{01} is the reference temperature for static loading (°C), and dK_c/dt is the rate of change of the stress intensity factor [(MPa-√m)/s]. The parameter Γ is given in Figure 7.

$$\Gamma = 9.9 \exp \left[\left(\frac{T_{01}}{190} \right)^{1.66} + \left(\frac{F_y}{722} \right)^{1.09} \right]$$

Source: Reference 6

Figure 7. Equation. Additional loading rate equation parameter.

In this equation, F_y is the static yield strength (MPa). To determine the shift in reference temperature for a dynamic loading rate, the applied stress was assumed to be applied over a period of 0.5 seconds (approximate time for a truck traveling at 60 mph to reach the middle of a 100-ft simple span), and dK_c/dt was calculated using this loading period and the calculated stress intensity factor.

To incorporate the variation in fracture toughness at a given temperature, the cumulative probability of fracture, P_f , was taken as a probabilistic input. The service temperature was assumed as -30°F, the Lowest Anticipated Service Temperature (LAST) for AASHTO Zone 2.

STRESS INTENSITY FACTORS

The stress intensity factor for this study was taken as presented in Figure 8.

$$K_I = Y\sigma\sqrt{\pi a}$$

Source: Reference 7

Figure 8. Equation. Stress intensity factor.

In this equation, σ is the applied tensile stress (including dead and live load stresses), a describes the size of the flaw in the member, and Y is a combination of factors accounting for the flaw and member geometry. Two different flaw geometries were considered, a through-thickness edge crack, and a semi-elliptical embedded flaw, both shown in Figure 9. These flaws were chosen to represent a wide range of common flaws in steel bridges.

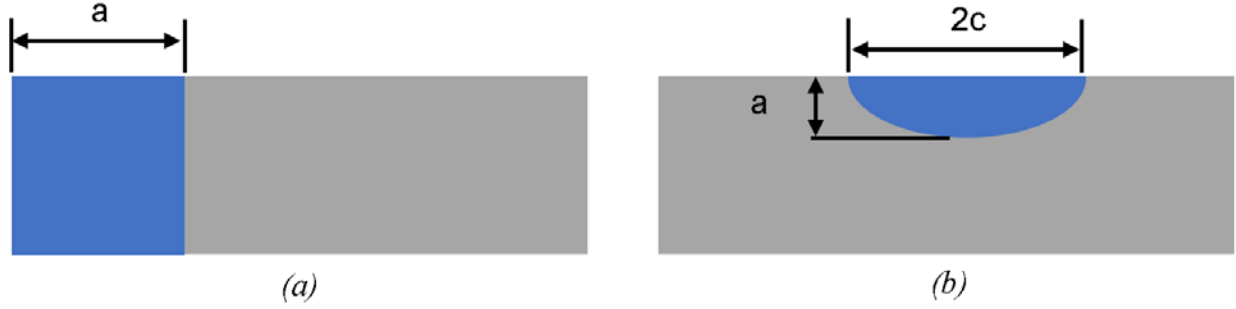


Figure 9. Illustration. Assumed cracks: (a) through-thickness, and (b) semi-elliptical.

For the edge crack, Y was set equal to 1.12, a free-surface correction factor.⁽⁷⁾ For the semi-elliptical crack, Y was taken as shown in Figure 10.

$$Y = 1.12M_k \sqrt{\frac{1}{Q}}$$

Source: Reference 7

Figure 10. Equation. Stress intensity correction factor.

In this equation, M_k is the back-surface correction factor, Q is the elliptical flaw shape parameter, and the factor of 1.12 is the free-surface correction factor. The back-surface correction factor, which accounts for an increase in stress intensity when the flaw depth approaches the back surface of the cracked medium, is given in Figure 11.

$$M_k = \begin{cases} 1 & \frac{a}{B} < 0.5 \\ 1 + 1.2 \left(\frac{a}{B} - 0.5 \right) & \frac{a}{B} \geq 0.5 \end{cases}$$

Source: Reference 7

Figure 11. Equation. Back surface correction factor.

In this equation, B is the thickness of the cracked medium. The elliptical flaw shape parameter, Q , is given in Figure 12.

$$Q = \Phi^2 - 0.212 \left(\frac{\sigma}{F_y} \right)^2$$

Source: Reference 7

Figure 12. Equation. Elliptical flaw shape parameter.

In this equation, Φ is the complete elliptical integral of the second kind (determined from the elliptical depth-to-width ratio through curve fitting) and F_y is the yield strength of the material. For simplicity, a depth-to-width ratio ($a/2c$) of 0.25 was assumed for all semi-elliptical flaws within this study.

The flaw sizes for this study were assumed as deterministic, and plots were constructed of reliability index vs. flaw size for different steels and different material thicknesses. This was done as no sufficient database for inherent flaw sizes in steel bridge members could be identified for determining a probabilistic distribution of flaw sizes to use within the calculations.

APPLIED STRESSES

The applied dead and live load stresses acting on the member were treated as random variables, with normal distributions and bias factors and coefficients of variation (COVs) based on NCHRP Report 386.⁽⁸⁾ The bias factor for live load (LL) stress was based on the tabulated value for 100-ft simple span moment and 1-month maximum. The COV for LL stress was based on the tabulated value for any spans longer than 30 ft (100 ft span was assumed). These values were chosen to represent a common highway bridge.

Mean dead load (DL) and LL stresses were calculated assuming 1) that the flaw occurred in the tension flange of a girder, where the Strength I factored stress was set equal to the factored resistance of the tension flange, i.e. the factored yield strength, and 2) that the DL-to-LL ratio was equal to 4. The parameters for the DL and LL stress distributions obtained under this system are presented in Table 1 for 42 ksi (ASTM A242) and 50 ksi (all others) materials.

Table 1. Normal distribution parameters for applied stresses.

Yield Strength (ksi)	Mean Dead Load Stress (ksi)	Std. Dev. Dead Load Stress (ksi)	Mean Live Load Stress (ksi)	Std. Dev. Live Load Stress (ksi)
42	24.16	1.93	5.66	0.62
50	28.77	2.30	6.73	0.74

MONTE CARLO SIMULATION

To account for the probabilistic inputs (applied DL and LL stresses and cumulative probability of fracture), a Monte Carlo Simulation (MCS) was conducted for each combination of material type, material thickness, flaw size, and flaw geometry. The proposed limit state function was used to determine if each set of random samples within the simulation would result in a fracture. The probability of failure was calculated by dividing the number of failures (cases where g was less than zero) by the total number of samples within the MCS. The distribution of g was assumed to be normal, and the reliability index was calculated as the negative inverse normal distribution of the probability of failure.

Preliminary simulations with a limited number of samples (50,000) were completed by M&M personnel using Microsoft Excel. Later, researchers at Lehigh University ran simulations with 5 million samples using Matlab. This number of samples was chosen based on a convergence study conducted by Lehigh which demonstrated that the reliability indices calculated from the simulations did not change significantly with a different set of random samples when 5 million samples were used.

RESULTS

MASTER CURVE REFERENCE TEMPERATURE

The MC reference temperatures for the selected materials are presented in Table 2. As expected, the reference temperatures for modern steels are lower than for the legacy steels, indicating that they have better fracture toughness than the legacy steels.

Table 2. Master curve reference temperatures for selected materials.

Material	T₀ (°F)
Legacy A242	12.27
Legacy A572	-8.52
Modern A709-50	-81.62
Modern A709-50W	-180.2
Modern A709-HPS50W	-54.29

Using these reference temperatures, the master curve can be used to determine the mean fracture toughnesses and their variations for each material. A comparison of the variations in each material at a temperature of -30°F is presented in Figure 13. The A709-50W steel, while having similar lower bounds to the other steels, has a much higher average and upper bound than the other steels. Interestingly, the HPS grade has the lowest average and upper bound out of the modern steels. As previously discussed, producers are free to adjust their chemistries within the boundaries of ASTM A709, and as such, different properties are possible across different producers. Accordingly, HPS grades of one producer may have lower toughnesses than non-HPS grades of a different producer, as is the case here. This does not indicate that the HPS steel is in any way deficient; it does however indicate that some manufacturers are achieving larger toughnesses than typical HPS steels in their non-HPS grade steels without specifically attempting to do so.

RELIABILITY BY MATERIAL GRADE

The results organized by material grade but with differing flaw shapes and flange thicknesses are presented in Figure 14 through Figure 18. Each figure contains a family of curves showing the variation in reliability index with crack size for different crack shapes and material thicknesses, but all having the same material. The results show a decreasing reliability index with increasing crack size for all materials as expected. In addition, the edge crack cases, with larger stress intensity, generally have lower reliability than for the semi-elliptical crack cases. The reliability index is generally lower for the 2.5-inch thick components than the 1-inch thick components, due to the reduction in fracture toughness for thicker materials. For the semi-elliptical cracks in 1-inch thick plates, there is a change in slope of the curve for greater than 0.5-inch crack size, due to the increase in stress intensity from the crack approaching the back surface.

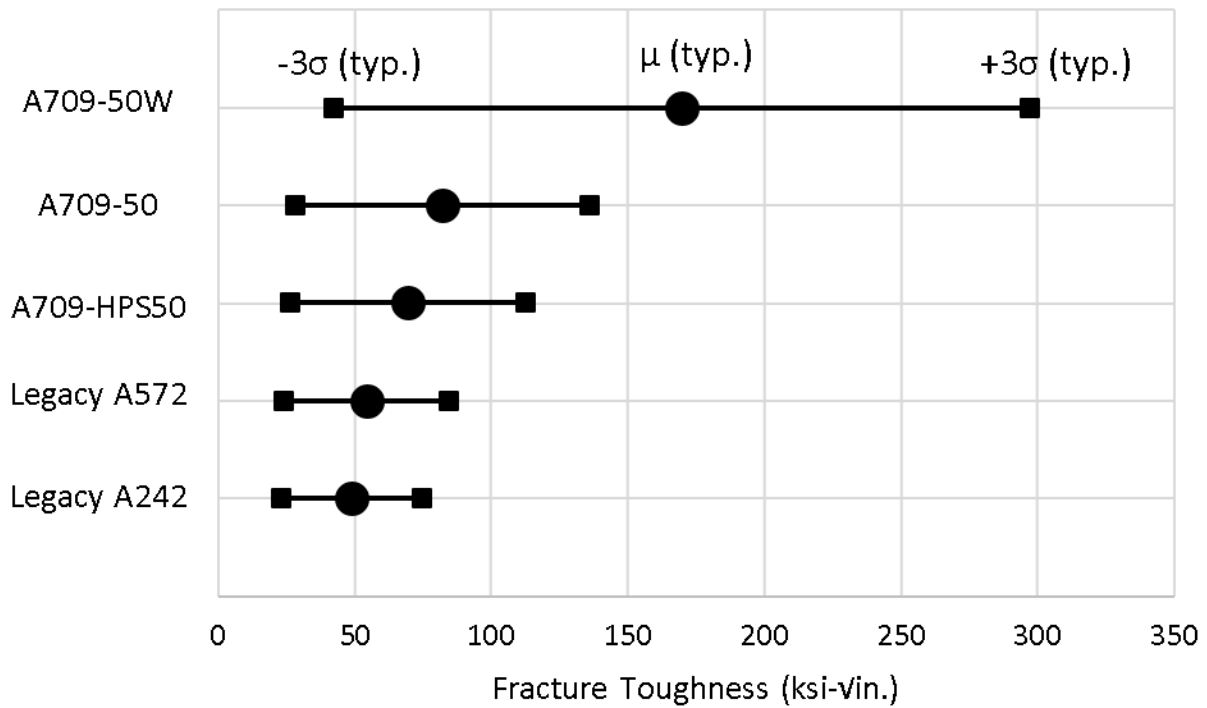
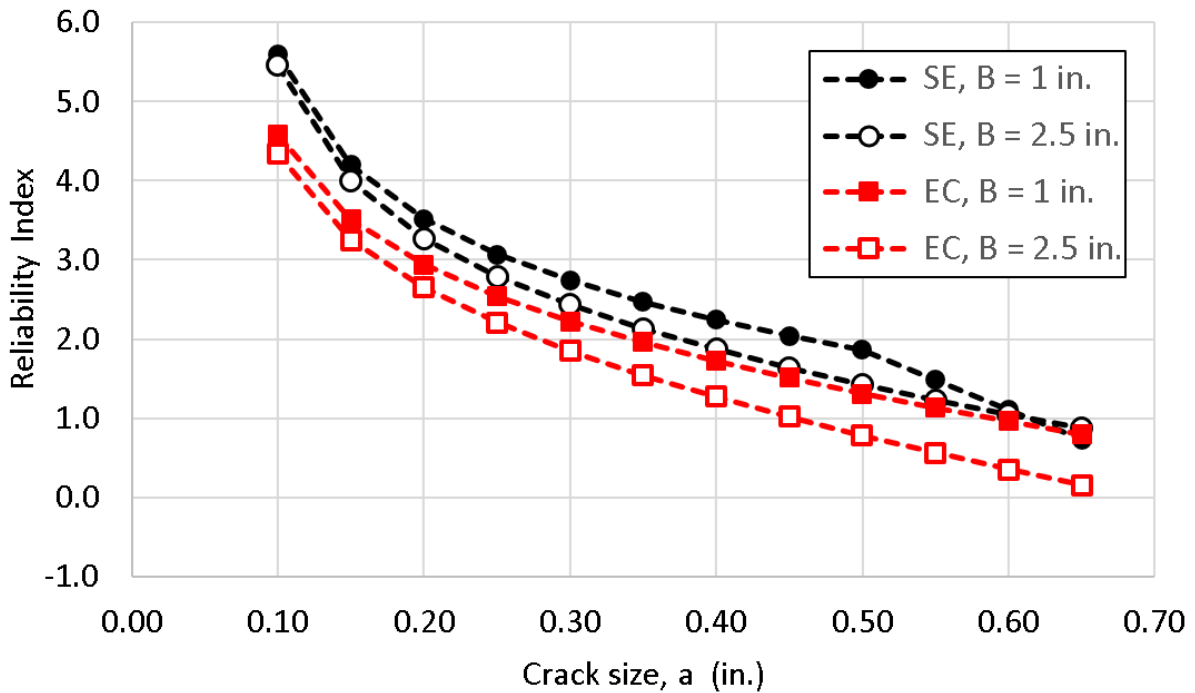


Figure 13. Graph. Variability in fracture toughness at -30°F for legacy and modern steels.



Note: SE denotes semi-elliptical crack, EC denotes through-thickness edge crack, B is material thickness

Figure 14. Graph. Simulation results for a legacy ASTM A242 steel.

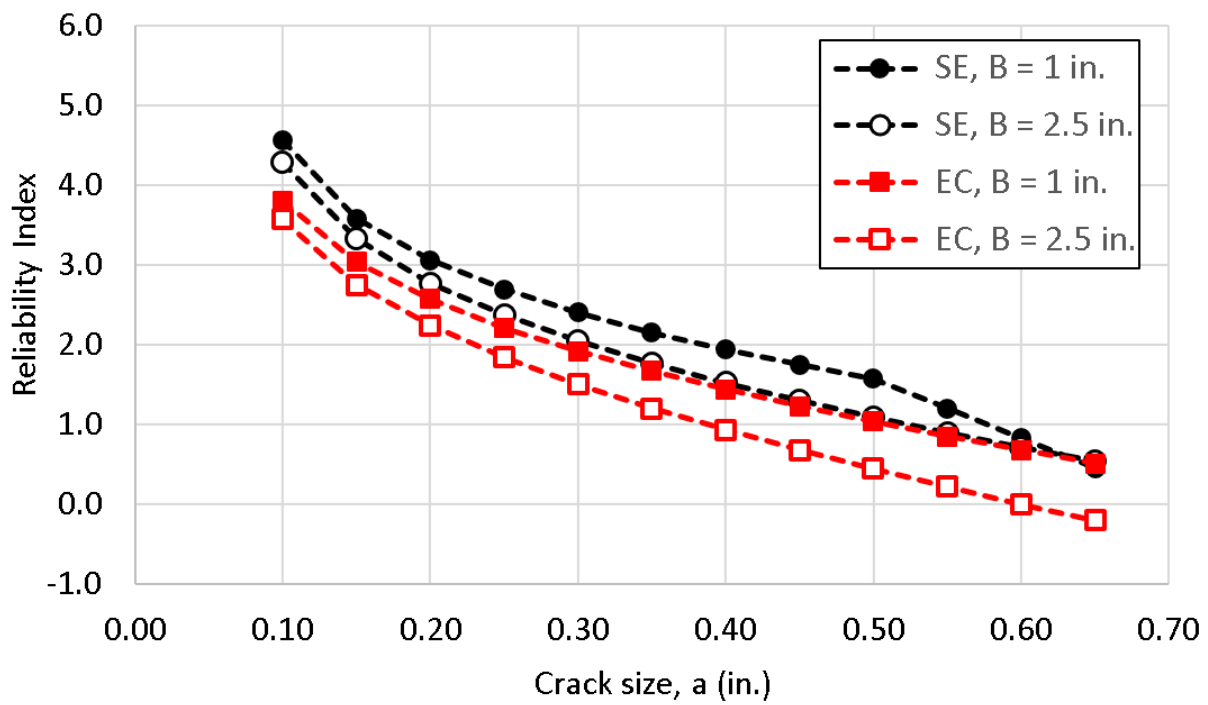


Figure 15. Graph. Simulation results for a legacy ASTM A572 steel.

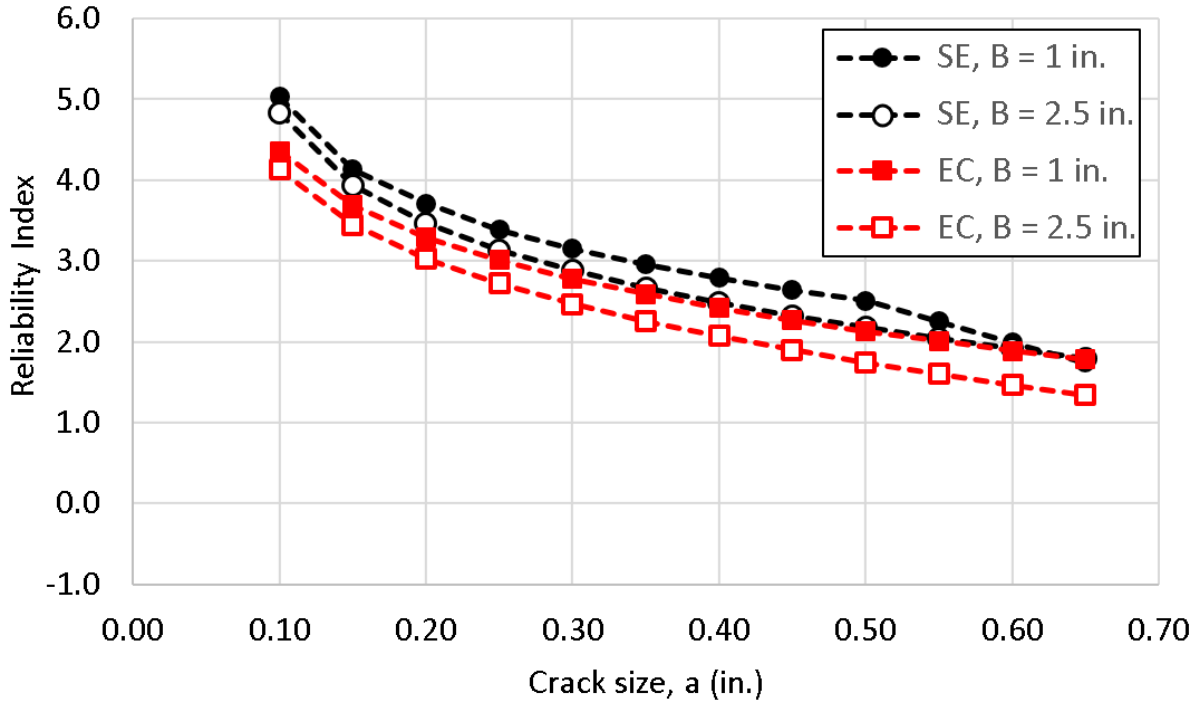


Figure 16. Graph. Simulation results for a modern ASTM A709-50 steel.

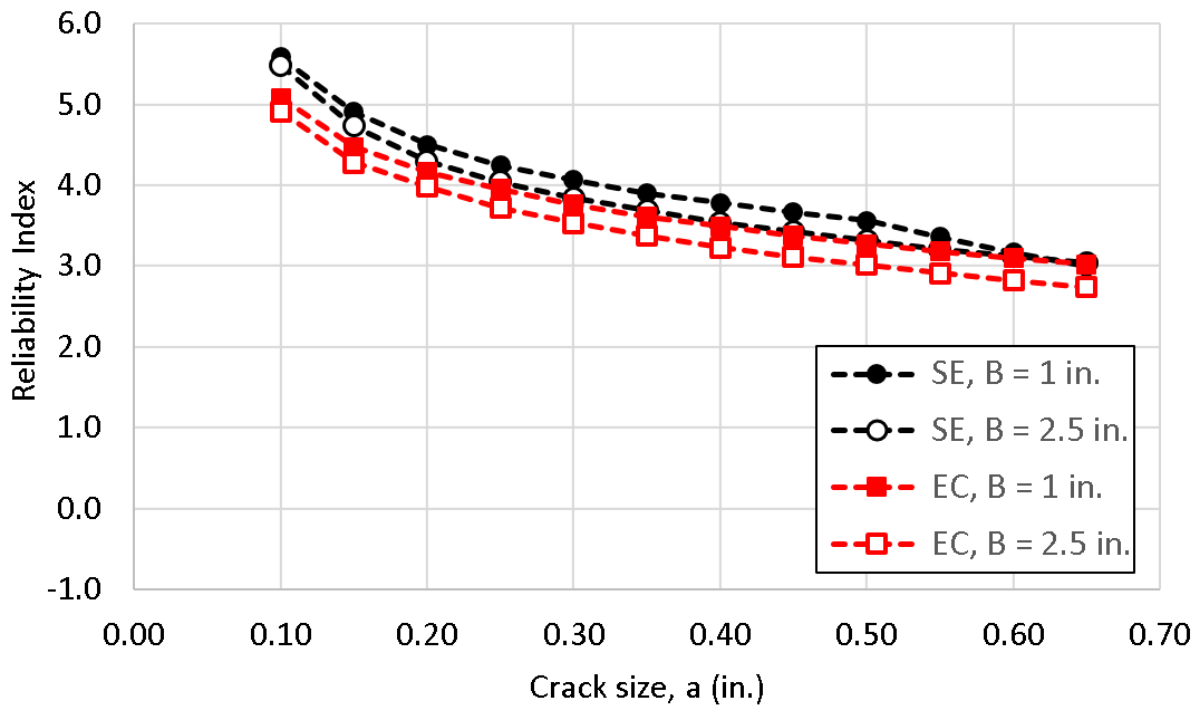


Figure 17. Graph. Simulation results for a modern ASTM A709-50W steel.

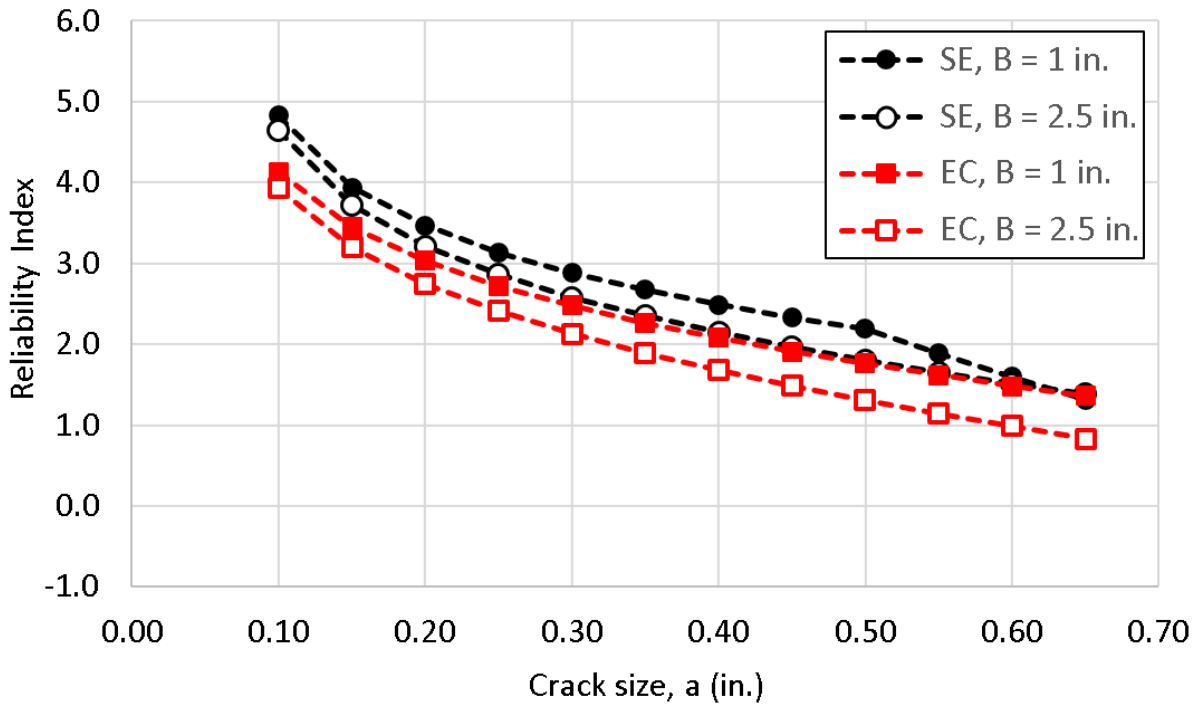


Figure 18. Graph. Simulation results for a modern ASTM A709-HPS50W steel.

The maximum crack sizes for achieving a reliability index of 3.5 (the target reliability for the AASHTO strength limit states) for each combination of material, thickness, and crack shape are shown in Table 3. This reliability index is met only at the smallest crack sizes (approximately 0.14 inch or 5/32 inch for modern steels). Fortunately, cracks of this size that may be present in new fabricated steel are larger than the rejectable crack sizes in AWS D1.5⁽⁹⁾ of between 0.01 inch (0.25 mm) and 0.09 inch (2.3 mm) depending on the arrangement of the crack. As evidenced by the figures, the reliability index falls below 3.5 as the crack size increases and may fall below zero (indicating greater than 50% probability of failure) for edge cracks in thicker plates of legacy steels.

Table 3. Maximum crack size (*a*) for target reliability index of 3.5.

Material	SE	SE	EC	EC
	B = 1 inch (inch)	B = 2.5 inch (inch)	B = 1 inch (inch)	B = 2.5 inch (inch)
Legacy A242	0.20	0.18	0.15	0.14
Legacy A572	0.16	0.14	0.12	0.10
Modern A709-50	0.23	0.20	0.17	0.15
Modern A709-50W	0.52	0.42	0.40	0.31
Modern A709-HPS50W	0.20	0.17	0.15	0.13

RELIABILITY BY CRACK TYPE AND MATERIAL THICKNESS

The results presented by crack type and material thickness with differing material types are presented in Figure 19 through Figure 22. Many of the same patterns can be observed in these plots as in the previous plots, namely the decreasing reliability index with increasing crack size. The reliability index is higher for modern HPS50W steel than for the legacy steels, with more benefit gained as the crack size increases. At a crack size of 0.65 inch, for example, the reliability index is more than doubled for all combinations of crack shape and material thickness, indicating a much lower probability of failure for larger cracks in modern steels than for legacy steels. However, at the minimum considered crack size (0.15 inch) the increase in reliability index is much smaller, on the order of 15% from legacy to modern steels with similar yield strengths (A572 and A709). This effect occurs due to the square root on the crack size in the stress intensity factor equation. Due to this equation, at smaller crack sizes the reliability depends more so on the stress intensity factor (the demand) than the fracture toughness (the resistance). As the crack size increases, the effect of the stress intensity factor becomes comparatively less, and the differences in fracture toughness and its effect on the reliability index become more pronounced.

Surprisingly, the reliability for A242 steel is higher than for A572 steel, even though A572 has slightly higher average toughness. This is due to the assumption that the stress is equal to the Strength I design stress, which means that the stress intensity (dependent on the applied stress) is generally lower for the lower yield strength A242 steel than for the A572 steel. Additionally, the A709-HPS50W steel has lower reliability than the non-HPS A709-50 and A709-50W. This is due to the materials having different manufacturers. Other than maintaining the minimum CVN

requirements as per AASHTO and ASTM standards, large variations in properties above these minimums are possible between manufacturers, as is visible here and previously in this report.

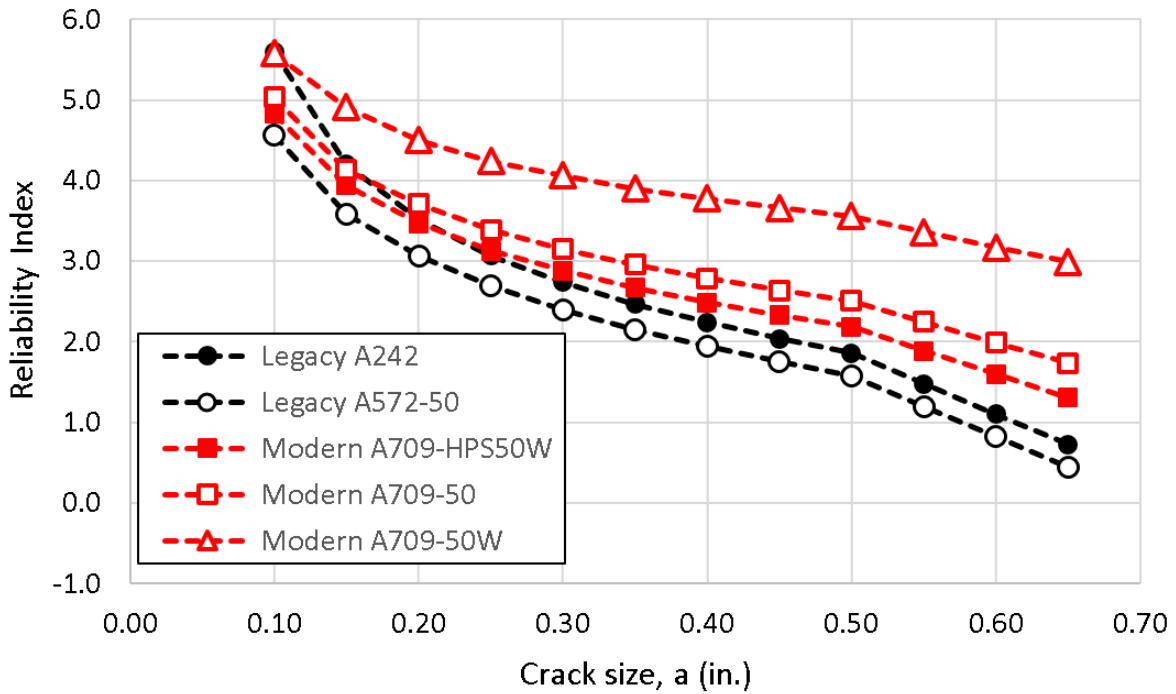


Figure 19. Graph. Simulation results for semi-elliptical crack in 1-inch thick component.

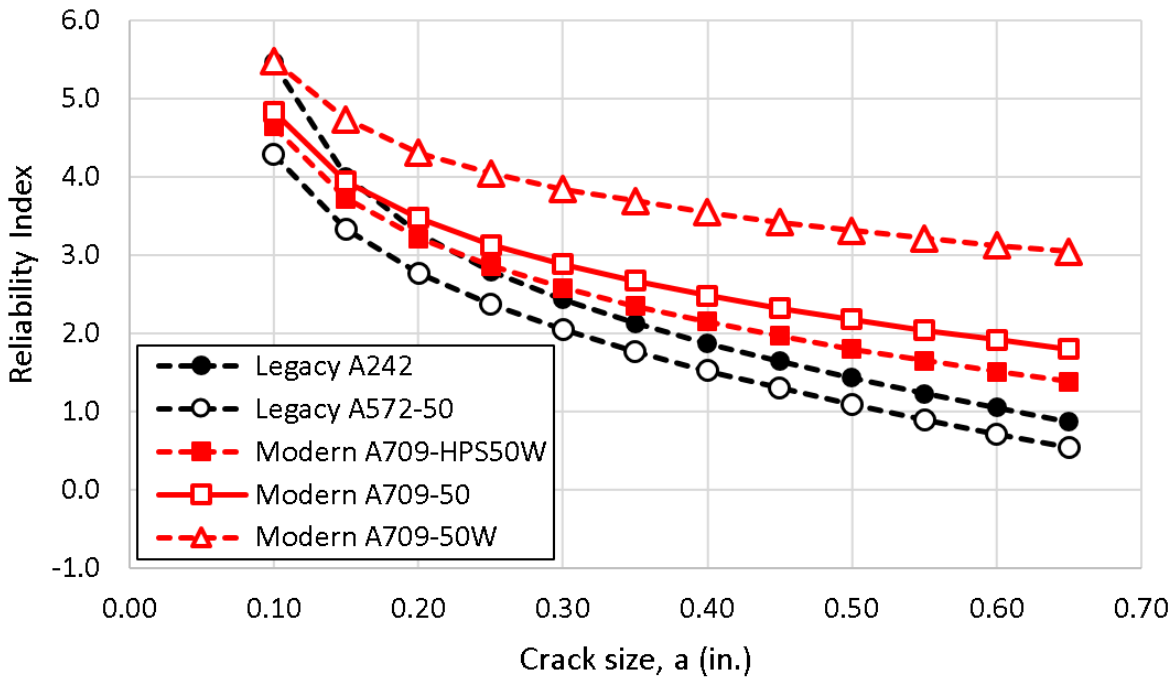


Figure 20. Graph. Simulation results for semi-elliptical crack in 2.5-inch thick component.

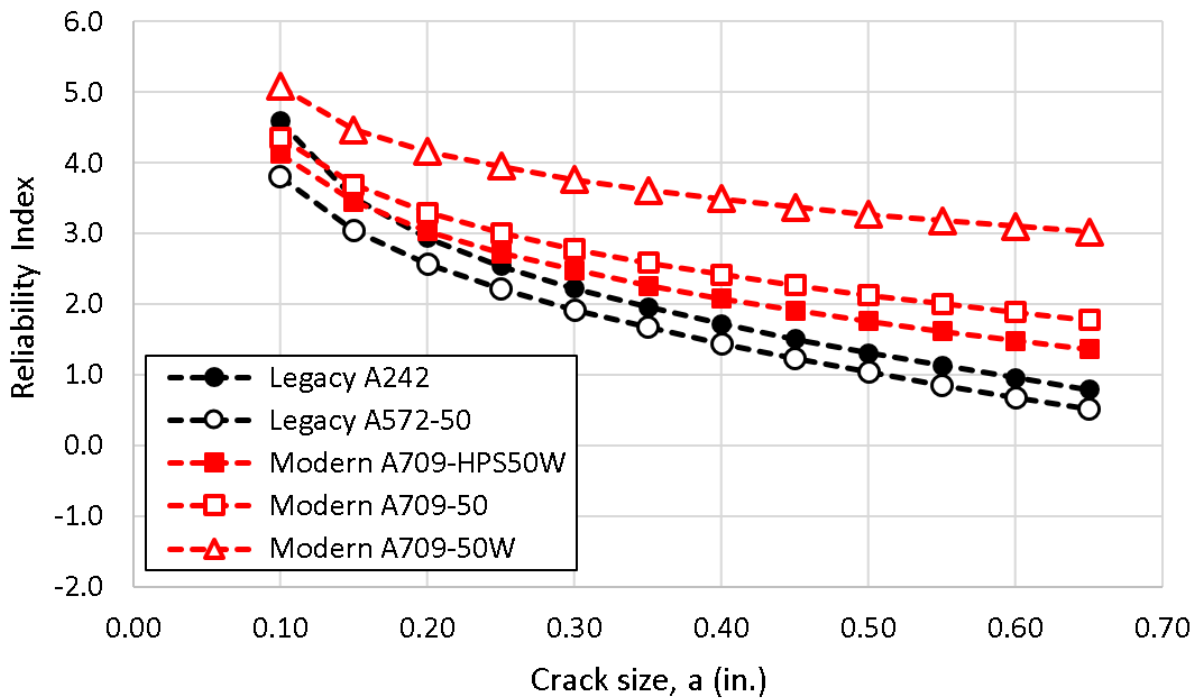


Figure 21. Graph. Simulation results for through-thickness crack in 1-inch thick component.

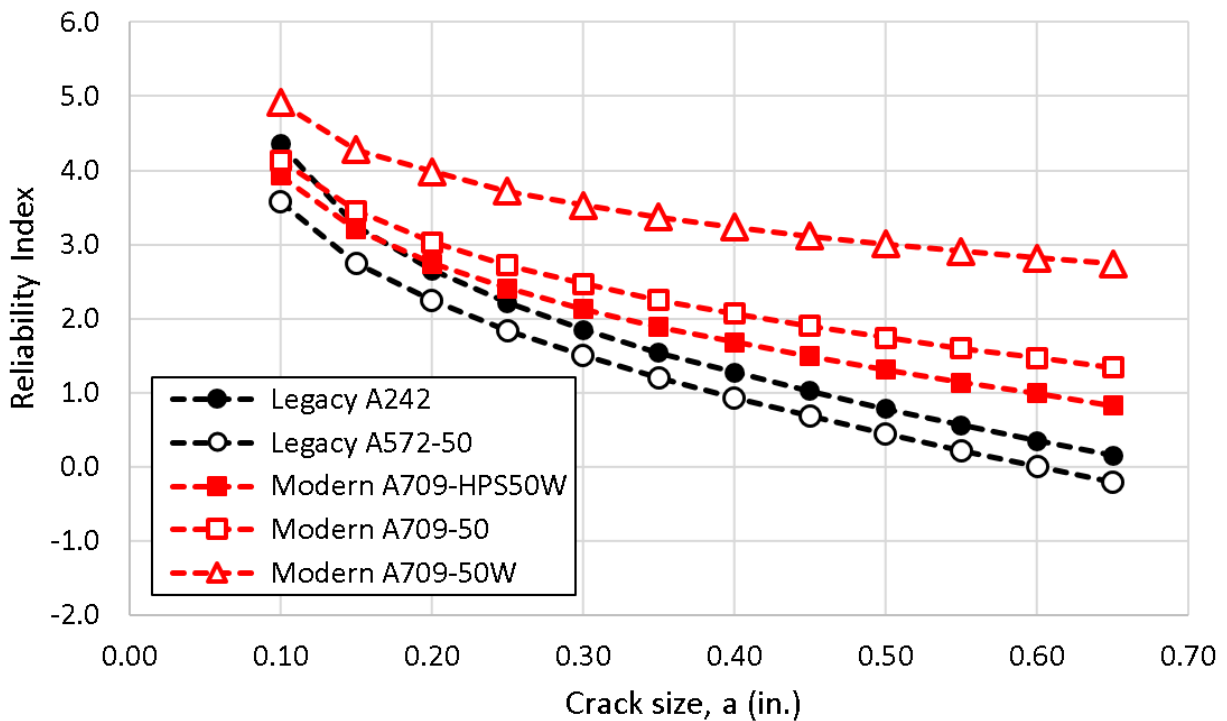


Figure 22. Graph. Simulation results for through-thickness crack in 2.5-inch thick component.

Overall, these results indicate that the use of steels with modern fracture toughnesses has two main benefits. First, the reliability against fracture is slightly higher for small crack sizes which might be expected to be present in new fabricated steel. Second, the reliability against fracture remains much higher than legacy steels even when significant cracks (greater than 0.5-inch size) are present in the material, such as fatigue, corrosion, or damage-related cracks that may form after years of service due to poor detailing practice or misuse of the structure. For example, given a 1 inch thick flange with semi-elliptical crack of 0.60 inch depth, the probability of failure for a bridge constructed of 50 ksi A572 steel is approximately 16%, where the probability of failure is approximately 5% for a similar bridge constructed of the A709-HPS50W steel examined in this study, and approximately 0.1% for a bridge constructed of the A709-50W steel examined in this study.

ADDITIONAL SIMULATIONS FOR LARGE TOUGHNESS STEEL

During the material gathering phase of the project, a steel supplier provided CVN data for a type of steel produced to the ASTM A709 standard but intended for use in cold environments. This steel, referred to as A709/A572 low carbon microalloyed steel, is commonly used in the fabrication of wind turbine towers and is currently limited to thicknesses of 2 inches or less. It is not known if any bridges have been constructed using this material. A preliminary study of the provided data indicated that the provided CVN values were on the upper shelf of the toughness transition curve, with approximately 260 ft-lb impact toughness at -30°F. This is in contrast with the other studied materials, which had values on the lower shelf or lower transition portion of the curve at low temperatures. Because of its very high average toughness and relatively low variability of toughness at low temperatures, this steel provides an excellent example of high toughness material that is currently available and could be utilized in bridge applications. Accordingly, simulations like those performed for the other steels were performed for this A709/A572 low C steel.

Given that the provided data was on the upper shelf, the master curve approach, which is intended for the lower shelf and transition region, was not applicable. Accordingly, a normal distribution of toughness at -30°F was assumed, with mean and standard deviation equal to 258.98 ksi-√in and 7.67 ksi-√in, respectively.

Preliminary Monte Carlo simulations revealed that the crack sizes for a target reliability index of 3.5 were much larger than those of the other steels, and that determining the reliability index for any small cracks would require too many samples to make further Monte Carlo simulation practical. With the assumption of a normal distribution for the fracture toughness and continued assumptions of normal distributions for all other stochastic variables, it was accordingly decided to use the Hasofer-Lind (HL) approach⁽¹⁰⁾ to determine the reliability indices as a function of crack size.

The HL approach is described in the following. For a limit state function of the general form shown in Figure 23, the Hasofer-Lind reliability index is shown in Figure 24.

$$g(\bar{x}) = a_0 + \sum_{i=1}^n a_i x_i$$

Source: Reference 10

Figure 23. Equation. General form of limit state function for Hasofer-Lind approach.

$$\beta_{HL} = \frac{a_0 + \sum_{i=1}^n a_i \mu_i}{\sqrt{\sum_{i=1}^n \sum_{j=1}^n a_i a_j \rho_{ij} \sigma_i \sigma_j}}$$

Source: Reference 10

Figure 24. Equation. General form of the Hasofer-Lind reliability index.

In these equations, a_i are constants defining the limit state function, x_i are the normally-distributed random variables contributing to the limit state function, μ_i and σ_i are the mean and standard deviation, respectively, of the random variables, and ρ_{ij} are the correlation coefficients for correlations between the random variables. For this case, the random variables are assumed uncorrelated, and the reliability index is presented in Figure 25.

$$\beta_{HL} = \frac{\alpha_0 + \sum_{i=1}^n a_i \mu_i}{\sqrt{\sum_{i=1}^n (a_i \sigma_i)^2}}$$

Figure 25. Equation. Hasofer-Lind reliability index for uncorrelated random variables.

Inserting the limit state function, the reliability index is shown in Figure 26.

$$\beta_{HL} = \frac{\mu_{Kc} - 1.12\sqrt{\pi a}(\mu_{DL} + \mu_{LL})}{\sqrt{\sum_{i=1}^n (a_i \sigma_i)^2}}$$

Figure 26. Equation. Hasofer-Lind reliability index for fracture limit state function.

In this equation, μ_{Kc} , μ_{DL} , and μ_{LL} are the mean fracture toughness, dead load stress, and live load stress, respectively, σ_{Kc} , σ_{DL} , and σ_{LL} are the standard deviations of the aforementioned random variables, and a is the deterministically assumed crack size. This equation assumes the crack is a through-thickness edge crack, as preliminary investigations showed that the crack sizes at a reliability index of 3.5 were too large compared to the thickness of material for the use of an assumed elliptical thumbnail crack to be practical.

The results of this reliability analysis are presented in Figure 27, compared with the highest resulting reliability curve of the previously considered materials (A709-50W). The results indicate a much higher reliability index for a given crack size, with no significant probability of failure until cracks more than 7 inches long are present in the base material. This is due to the large average toughness and relatively small variation in toughness of the A709/A572 Low C steel compared to the other investigated steels, as presented in Figure 27. The high average and low variation in the A709/A572 Low C steel is due to the steel being at the upper shelf toughness for the considered temperature. In the transition region with decreasing temperature, the average toughness falls, and the variation increases. Eventually, as the steel enters the lower shelf region, the average toughness is very low and the variation continues to decrease until there is not much variation in toughness. Both the increased variation in the transition region and low variation on the lower shelf are visible in Figure 28 for the other considered steels.

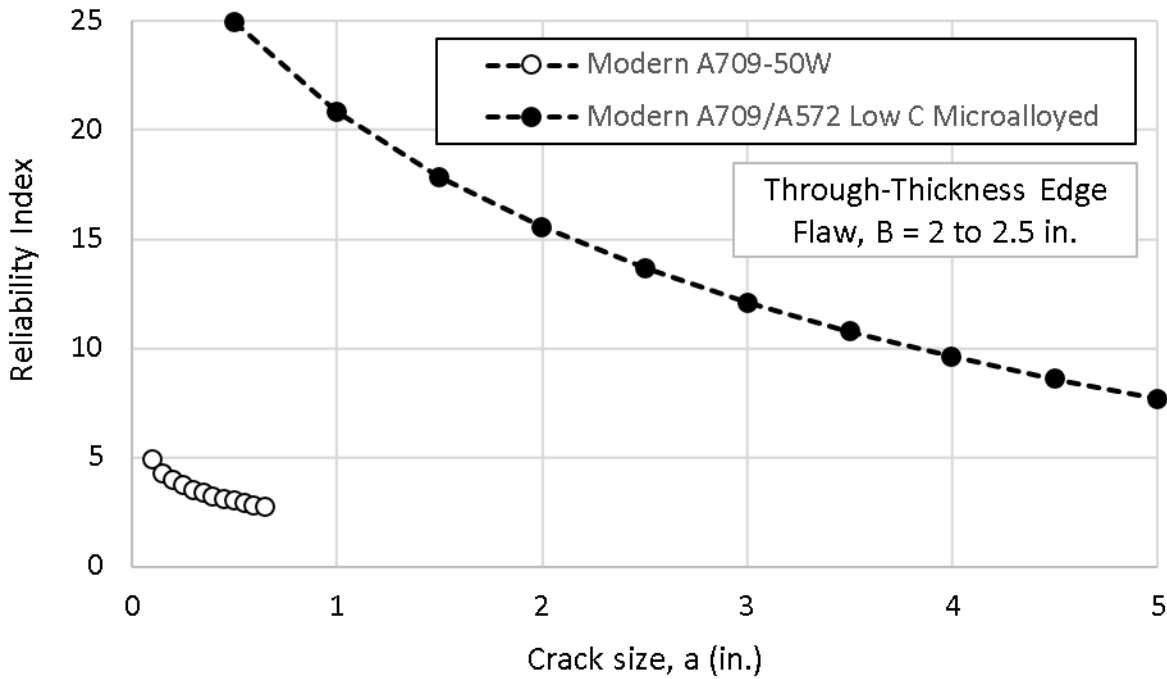


Figure 27. Graph. Hasofer-Lind reliability analysis results for modern A709/A572 low carbon microalloyed steel compared with modern A709-50 Monte Carlo simulation results.

These results indicate that an achievable high-toughness bridge steel could virtually eliminate sudden fracture as a failure mode for most typical bridges. With toughness on the upper shelf, the failure mode essentially shifts from a brittle fracture mode to a ductile tension fracture mode on the net section, which is a more desirable failure mode. As previously mentioned, the low C micro-alloyed steel investigated as part of this study is readily available, but it is currently only available in thicknesses up to 2 inches (50 mm). Further development would be required to develop a similar type of high-toughness steel in larger thicknesses.

The Hasofer-Lind methodology may also be extended to fictitious steels to obtain a better understanding of what upper-shelf fracture toughnesses would be required to obtain a target reliability index of 3.5. Figure 29 shows assumed distributions of fracture toughness for four synthetic/fictitious steels in addition to the real A709/A572 Low C microalloyed steel. These synthetic distributions were obtained by fixing the lower bound of the toughness (mean minus three standard deviations) to 200, 150, 100, and 50 ksi- $\sqrt{\text{in}}$ for synth materials 1 through 4, respectively. For simplicity, the standard deviation was assumed as that of the A709/A572 low C steel.

The results simulations for each of the materials assuming through-thickness cracks, the same stresses as previous simulations, and the assumed toughness distributions are presented in Figure 30 as plots of reliability index vs. critical crack size. These plots demonstrate similar trends as the previous simulations performed as part of this study, namely that larger reliability is achieved when toughness is increased. In this case, where the overall variability in toughness is held constant while the lower bound toughness is varied, the largest improvements in the reliability

index are observed at the smallest crack sizes, although there are improvements at all crack sizes. Even a moderate increase in fracture toughness would allow for an excellent improvement in reliability and critical crack size prior to ultimate failure (as presented in Figure 31).

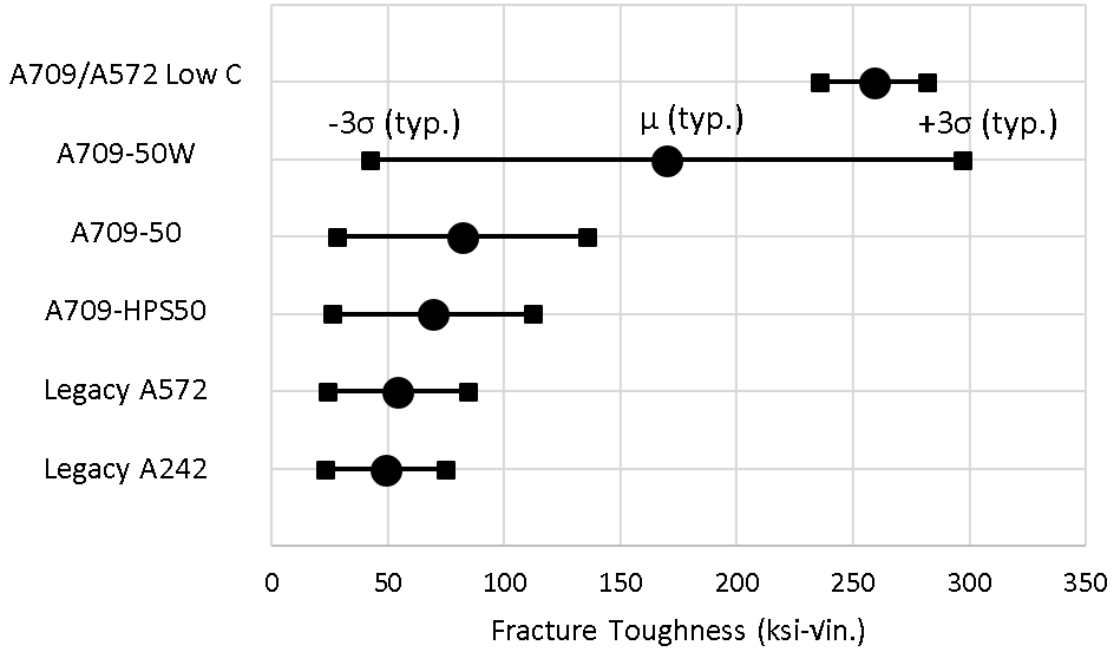


Figure 28. Graph. Variability in fracture toughness at -30°F for all considered materials.

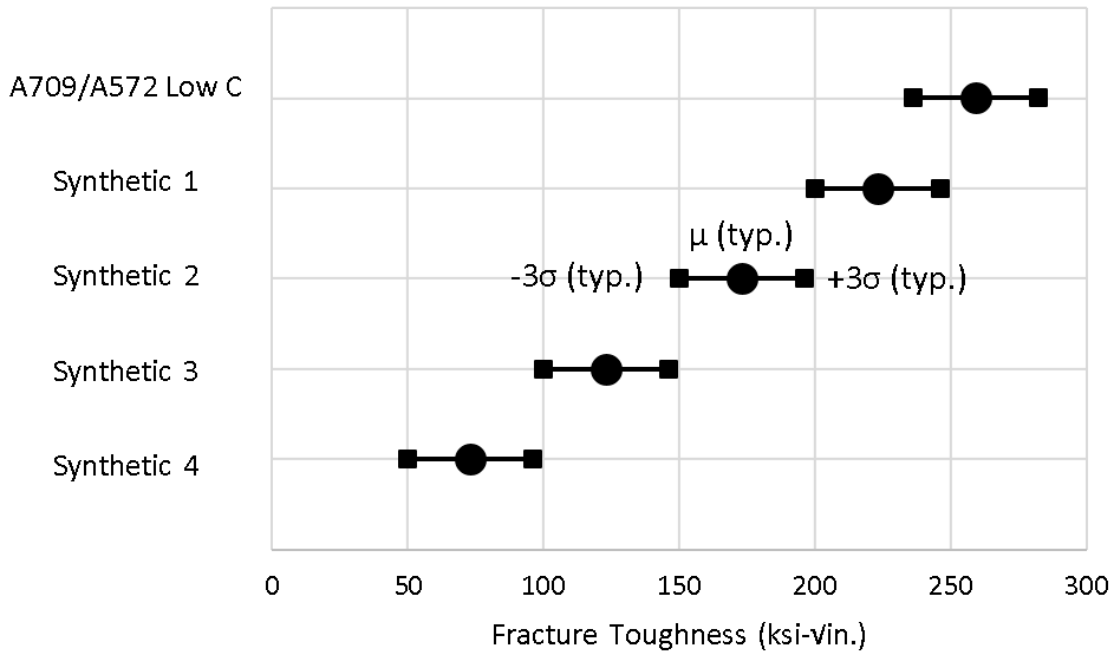


Figure 29. Graph. Variability in fracture toughness at -30°F for synthetic/fictitious steels, compared to variability for A709/A572 low C steel.

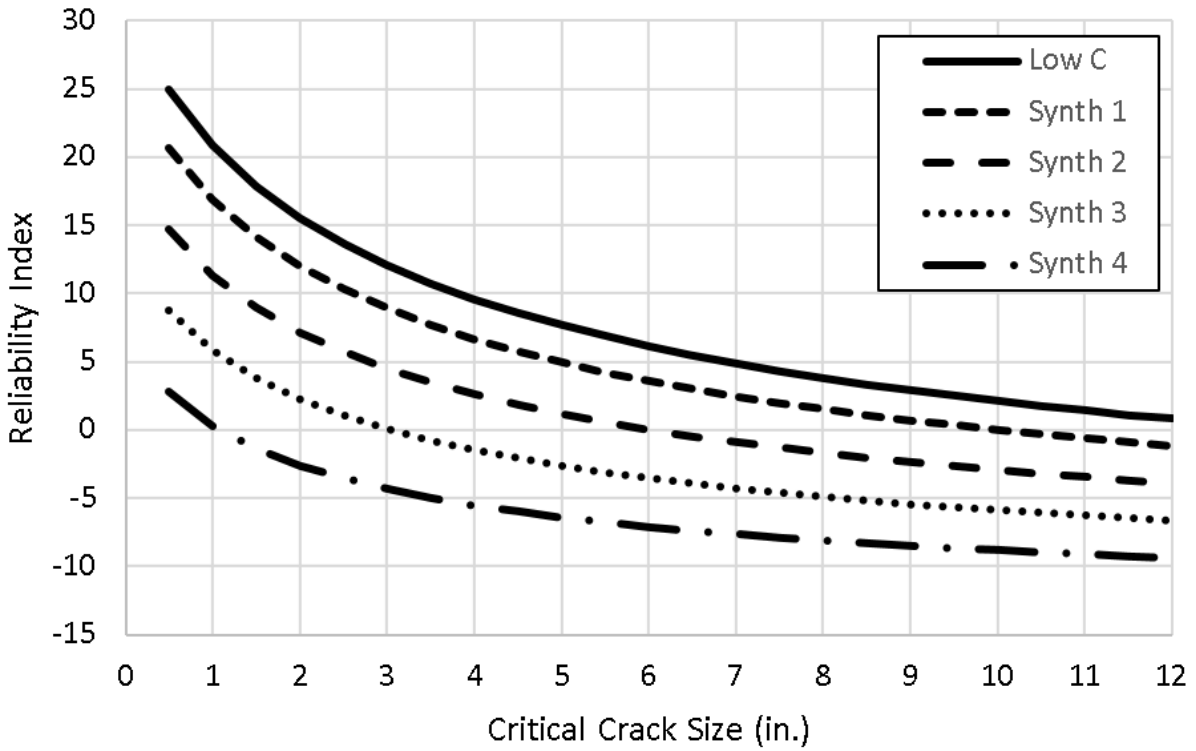


Figure 30. Graph. Reliability index vs. critical crack size for synthetic materials.

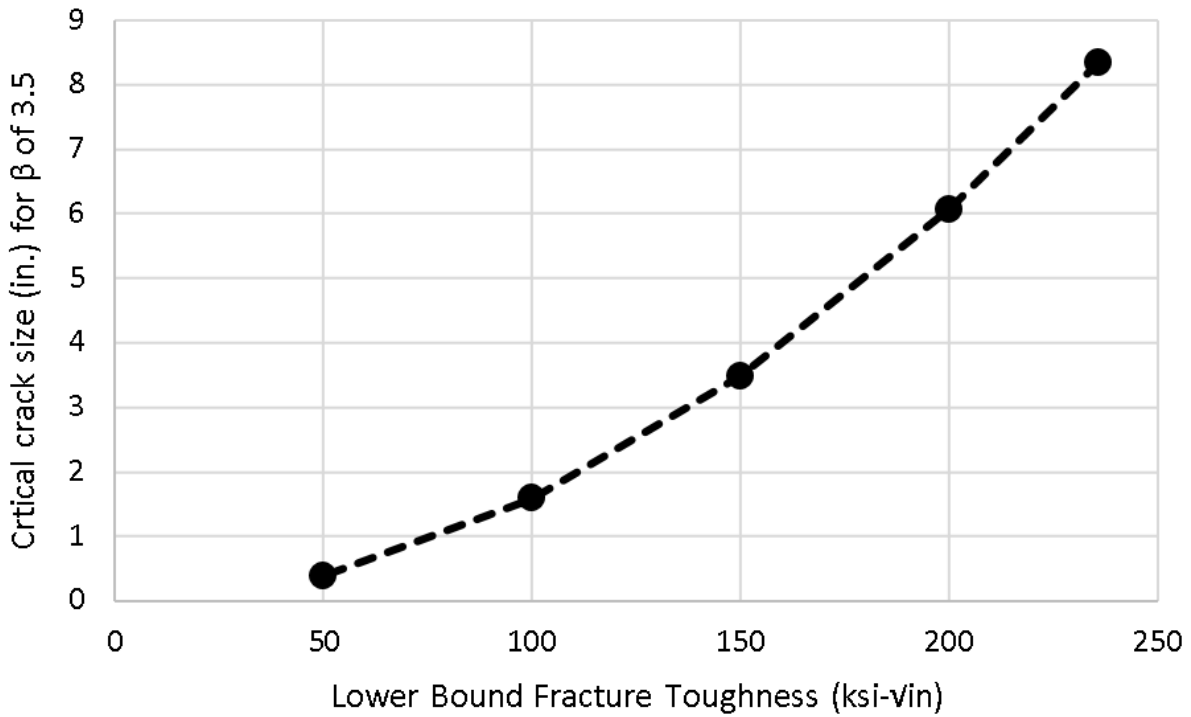


Figure 31. Graph. Critical crack size vs. lower bound fracture toughness for β of 3.5

The synthetic analysis runs presented in the preceding paragraphs and figures imply that an enforcement of higher minimum toughnesses may be beneficial for decreasing the fracture risk of steel bridges. Higher toughnesses would be effective in increasing the reliability of steel bridges with respect to brittle fracture in two ways, both of which are made possible by the large increase in critical crack size before the occurrence of brittle fracture. First, if the decrease in cross-sectional area due to the crack growth is large enough relative to the difference between gross and net area of the section, the failure mode of the member may shift from brittle fracture to ductile fracture over the net section. This shift is from a sudden, hard-to-predict failure with little or no warning to a more gradual failure that can be better predicted and responded to by bridge owners. Second, the larger critical crack sizes may allow more time for inspectors to find and locate growing fatigue cracks before they reach critical size. This however, depends on the size of the crack relative to the member, as the fatigue crack growth rate accelerates rapidly as the size of the crack approaches the size of the member.

While larger toughnesses would certainly help in reducing the fracture risk of steel bridges, it is difficult to say at this time how much of an increase in fracture toughness or CVN impact energy would be required. To determine updated requirements which could take advantage of high toughness steels already on the market, a target reliability would have to be established for the fracture limit state. Additionally, maximum allowable flaw sizes would have to be determined, which are related to the choice of a target reliability. Research and literature review on a sufficient fracture toughness-CVN impact energy correlation for upper shelf behavior would also be required. Finally, a larger survey of currently marketed steels and their toughnesses would assist in the above tasks.

CONCLUSIONS

Through the results of this study, the following conclusions have been reached. First, a limit state equation has been developed based on LEFM, which provides a quantifiable approach to calculate the reliability of steel bridge members to fracture failure. This limit state was used to determine that the fracture reliability for modern bridge steels is generally consistent with the target reliability of AASHTO LRFD strength limit states. The main benefit of modern steels appears to be in providing much greater reliability against fracture that may occur from developing fatigue cracks. A secondary benefit of these steels is in providing greater reliability against fracture if a crack is discovered during the routine inspection process, or if it goes undetected. In addition, the rapidly decreasing reliability against fracture with larger crack sizes validates the current practice of remedying/removing cracks when they are first discovered, rather than monitoring and assuming there is time to failure.

Further research on the current ASTM A709 bridge steels on the market and how their toughnesses vary from manufacturer to manufacturer would be useful for determining upgraded minimum CVN impact toughnesses for immediate implementation in the AASHTO LRFD Bridge Design Specifications.

Steels are available on the market, such as the low C A709/A572 presented in this study, which provide high enough fracture toughness at low temperatures to essentially eliminate brittle fracture as a plausible failure, shifting the failure to a ductile fracture on net section (when the ultimate strength of the material on the reduced section is exceeded). Such steels provide great motivation for future study in this area aiming to determine enhanced minimum toughness requirements for implementation in the Fracture Control Plan. Exploratory analyses performed within this report on synthetic (i.e. fictional) steels with toughnesses ranging between current ASTM A709 bridge steels and the A709/A572 low carbon microalloyed steel have indicated that even moderate increases in the toughness of A709 would be highly beneficial. Further research should be performed to determine the necessary minimum toughness requirements to essentially eliminate brittle fracture as a plausible failure mode in newly constructed steel bridge members. This is currently difficult to accomplish with available information and would require the determination of a target reliability for the fracture limit state, a better upper-shelf correlation between fracture toughness and CVN impact toughness, and a wider range of experimental data and testing.

REFERENCES

1. AASHTO. (2014). *AASHTO LRFD Bridge Design Specifications*. 7th ed. American Association of State Highway and Transportation Officials, Washington, DC.
2. Collins, W., Sherman, R., Leon, R., & Connor, R. (2016). State-of-the-art fracture characterization. I: Master curve analysis of legacy bridge steels. *ASCE Journal of Bridge Engineering*, 21(12), 04016097.
3. Artmont, F.A., Adams, A.R., Murphy, T.P., Hopper, T., & Connor, R.J. (2018). Material Testing and Forensic Investigation of the Full-Depth Truss Chord Fracture in the Delaware River Turnpike Toll Bridge. *Proceedings of the 2018 International Bridge Conference*.
4. Roberts, R., Irwin, G. R., Krishna, G. V., & Yen, B. T. (1974). *Fracture Toughness of Bridge Steels - Phase II Report* (No. FHWA-RD-74-59 Final Rpt.).
5. Barsom, J.M. (1975). Development of the AASHTO Fracture-Toughness Requirements for Bridge Steels. *Engineering Fracture Mechanics*, 7(3). 605-618.
6. Altstadt, S., Wright, W., & Connor, R. (2013). Proposed Revisions to the current Charpy V-notch requirements for structural steel used in US bridges. *ASCE Journal of Bridge Engineering*, 19(1), 131-140.
7. Barsom, J. M., & Rolfe, S. T. (1999). *Fatigue and fracture control in structures*. West Conshohocken, PA: American Society for Testing and Materials.
8. Nowak, A.S. (1999). *Calibration of LRFD Bridge Design Code*. NCHRP Report 386. Washington, D.C.: National Academy Press.
9. AASHTO/AWS (2015). AASHTO/AWS D1.5:2015 Bridge Welding Code.
10. Hasofer, A.M. & Lind, N.C. (1974). Exact and Invariant Second-Moment Code Format. *Journal of Engineering Mechanics*, 100(1), 111-121.



U.S. Department of Transportation
Federal Highway Administration

FHWA-HIF-18-047